Research Article　　　　　　　　　　　　　　　　　　　　　　　　　　**Open Access**

Effect of Chitosan-Stabilized Selenium Nanoparticles on Cell Cycle Arrest and Invasiveness in Hepatocarcinoma Cells Revealed by Quantitative Proteomics

Isabel Lopez-Heras[1], Raquel Sanchez-Diaz[1], Daniela S Anunciação[2], Yolanda Madrid[1], Jose L Luque-Garcia[1*], Carmen Camara[1]

[1]Department of Analytical Chemistry, Faculty of Chemistry, University Complutense of Madrid, Madrid, Spain
[2]Institute of Chemistry and Biotechnology, University Federal of Alagoas, Maceió, Brazil

Abstract

Selenium nanoparticles have been recently proposed as a potential chemotherapeutic agent due to its low toxicity and its ability to arrest the cell cycle of cancer cells. However, the biochemical mechanisms associated to this effect have not yet been uncovered. We evaluate here the potential of chitosan-stabilized selenium nanoparticles to induce cell cycle arrest and to inhibit in-vitro invasiveness in HepG2 cells. In addition, we use a quantitative proteomic approach to identify potential protein targets involved in the mechanisms associated to selenium nanoparticles exposure. Our data suggest that the induction of the cell cycle arrest at the S phase is mediated by de-regulation of the eIF3 protein complex. We found additional de-regulated proteins upon selenium nanoparticles exposure that could also be involved in the overall inhibition of cell proliferation. These findings not only support the potential of chitosan-stabilized selenium nanoparticles as anti-cancer therapy but also provide a deeper insight into the mechanisms associated to their chemotherapeutic effects.

Keywords: Selenium nanoparticles; Cell cycle arrest; SILAC; eIF3 protein complex; Inhibition of invasiveness

Introduction

Selenium is one of the essential trace elements and has great importance in nutrition and medicine due to its antioxidant properties. The relationship between selenium intake/status and several health outcomes such as cancer, cardiovascular disease, diabetes and male fertility have been recently reviewed [1]. It is known that the dose and the chemical form of selenium have a significant influence on these beneficial effects [2].

Selenium nanoparticles (SeNPs), which are considered a novel Se compound, are attracting increasing attention of the scientific community due to their excellent antioxidants properties and low toxicity in comparison with other Se-species such as selenomethionine (SeMet) [3], selenium methyl selenocysteine (SeMeSeCys) [4] and selenite (Se IV) [5]. It has also been reported that SeNPs exhibit a great selectivity between cancer and normal cells showing a broad spectrum of growth inhibition for A375, CNE2, MCF-7 and HepG2 cancer cells This effect was more pronounced than when using Se IV at a similar concentration [6]. Recently, it has also been shown the anti-proliferative effect of SeNPs on HeLa, MDA-MB-231 and HepG2 cells in a dose-dependent manner by induction of cell cycle arrest [7,8]. However, the biomolecular mechanisms involved in this inhibitory effect have not yet been fully understood.

Proteomics is a powerful tool for describing complete proteomes at the organelle, cell, organ or tissue levels. Among all the proteomic approaches available, quantitative strategies are particularly attractive, since they allow for identification of differentially expressed proteins by comparing proteomes as affected by different conditions [9]. In this way, the identification of changes in individual proteins or group of proteins associated with SeNPs exposure could help to gain insight into the mechanisms of action of these NPs. Between the different alternatives for relative protein quantitation, stable isotopic labeling by amino acids in cell culture (SILAC) is one of the most reliable alternatives [10].

In this work, we investigated the potential cytotoxic effects of chitosan-stabilized selenium nanoparticles (Ch-SeNPs) and the biological mechanisms involved in the interaction of Ch-SeNPs with a human hepatocarcinoma (HepG2) cell line. We evaluated key parameters such as cellular viability, cellular uptake and localization, apoptosis and cell cycle pattern. In addition, we used SILAC for the identification of specific protein targets affected upon Ch-SeNPs exposure. Our data allowed us to dissect the mechanism by which Ch-SeNPs induce cell cycle arrest at the S phase. We conclude that Ch-SeNPs induced de-regulation of the eIF3 protein complex that affect the protein synthesis machinery inhibiting cell cycle progression. Finally, we demonstrated that exposure to Ch-SeNPs inhibit *in-vitro* invasiveness of HepG2 cells, thus supporting the idea of Ch-SeNPs as a potential chemotherapeutic agent [11].

Methods

Synthesis of Ch-SeNPs

Preparation of Ch-SeNPs was performed according to a previously described procedure [12] using chitosan polysaccharide as stabilizer and ascorbic acid as reducer. Synthesized Ch-SeNPs were stored at 4°C up to two months. Ch-SeNPs were characterized by TEM (see below).

Cell culture and treatment

Human hepatocarcinoma (HepG2) cells were maintained in Dulbecco´s Modified Eagle´s Medium (DMEM) supplemented with fetal bovine serum (10% v/v) and antibiotics in 5% CO_2 at 37°C. Ch-

SeNPs of 50-60 nm diameter were added at different concentrations ranging from 0.1 to 20 µg ml^{-1} and incubated for 48 h. Cells were then washed twice in phosphate-buffered saline (PBS) and harvested using 0.25% trypsin/0.1% EDTA.

Transmission electron microscopy analysis

For characterization of the synthesized Ch-SeNPs, droplets of the dispersion were placed onto a holey carbon film on copper grids. Micrographs were obtained using the JEOL 1010 JEM transmission electron microscope (JEOL) operating at 100 kV. Internalization of the NPs in HepG2 cells was observed after treatment with 1 µg ml^{-1} Ch-SeNPs for 48 h. Following exposure, attached cells were washed with PBS and fixed *in situ* with glutaraldehyde (2.5% v/v) and *p*-formaldehyde (4% v/v) in PBS at 4°C for 4 h. Cells were then washed and stored in PBS at 4°C overnight. After post-fixation with osmium tetroxide (1% v/v) for 1 h at room temperature and in the dark, the cells were dehydrated in graded ethanol series (from 30% to 100% ethanol) and harvested with propylene oxide. Cell suspensions were centrifuged at 1500 rpm for 30 seconds and the propylene oxide was removed. The pellets were treated with a mixture of resin:acetone and finally, treated with 100% resin. The resulting blocks were incubated at 65°C for 48 h until complete embedding. Ultrathin sections were cut, transferred onto copper grids and examined by TEM.

Cell viability assay

Cell viability was measured by the MTT assay. Briefly, cells were seeded in a 96-well plate at a concentration of 5x10^4 cells per well and exposed to Ch-SeNPs, Se IV or Ch-SeNPs synthesis media during 48 hours. 20 µl of 5 mg ml^{-1} MTT solution were added to the cells and incubated for 4 h at 37°C. Then, the media was removed and 100 µl of dimethyl sulfoxide was added. Absorbance was measured at 595 nm in a microplate reader.

Determination of internalized Ch-SeNPs by ICP-MS

Internalization of Ch-SeNPs was quantified in HepG2 cells exposed to 1 µg ml^{-1} Ch-SeNPs for 48 hours. After treatment, the exposure media, the PBS used for washing the cells and the cell pellet were digested in a microwave oven with a mixture of HNO$_3$ (65%) and H$_2$O$_2$ (35%) (2:1). Digested samples were appropriately diluted with distilled water and then Se was determined using an Agilent HP 7700x inductively coupled plasma-mass spectrometer (ICP-MS) (Agilent).

Flow cytometry analysis

Measurement of apoptosis in Ch-SeNPs and Se IV exposed cells was performed using an Annexin V-FITC kit (Sigma) following the manufacturer's instructions. Around 1x10^6 cells were treated with 1 µg ml^{-1} Ch-SeNPs for 48 hours. Then, cells were washed with PBS and re-suspended in 1 ml binding buffer solution at pH 7.5 containing HEPES/NaOH (100 mM), NaCl (1.4 M) and CaCl$_2$ (25 mM). Annexin V-FITC conjugate (5 µl) and propidium iodide (10 µl) were added to 500 µl of the cell suspension in order to label the apoptotic and necrotic cells, respectively. Cells were incubated in the dark at room temperature, and immediately examined using a FACScan flow cytometer (Becton-Dickinson). For evaluating the cell cycle arrest after exposure to Ch-SeNPs or Se IV, 1x10^6 HepG2 cells were re-suspended in 250 µl of PBS and mixed with an equal volume of a solution containing 60% ethanol (v/v) and 20 µg ml^{-1} of Hoechst 33258 reagent. Cells were incubated for at least 45 min at room temperature and the DNA content analyzed by flow cytometry.

Immunofluorescence assay

Cells were seeded onto cover slips and incubated with 1 µg ml^{-1} Ch-SeNPs for 48 h. Cells were washed with PBS, fixed with paraformaldehyde (4% v/v) in PBS for 10 min and permeabilized with Triton-X100 (0.1% v/v) in PBS for 15 min. Cells were blocked with bovine serum albumin (BSA, 2% w/v) for 1 h, followed by incubation with the primary antibody anti-eIF3a (1:100) (Bethyl) or anti-eIf3b (1:100) (BioLegends) for 40 min at room temperature on humid chamber. After three washings with PBS, cells were incubated with Alexa Fluor 586-labeled anti-rabbit IgG (1:1000) (Invitrogen) for 30 minutes at room temperature, followed by incubation with Alexa Fluor 488-labeled phalloidine (1:60) (Invitrogen) for 20 min at room temperature. Finally, VectaShield (Atom) was used for staining the nuclei with 4´,6-diamino-2-phenylindole (DAPI) and as a mounting media. Fluorescence microscopy was performed in a Motic AE31 epifluorescence microscope.

eIF3 gene knockdown

Human epithelial cervix carcinoma HeLa cells were seeded at 5x10^4 cells/well in 24-well plates and transfected with either eIF3 (30 pmol) or scrambled control siRNA (30 pmol) (Santa Cruz) using lipofectamine (Sigma) (1 µl) as transfection reagent and reduced serum media (opti-MEM) as transfection media. Cells were incubated in the transfection media for 5 h. The transfection was stopped by adding complete DMEM 10% FBS. After incubation for 24 h at 37°C 5% CO$_2$, the cells were harvested for further analyses.

Western blotting

Whole total lysates were separated by SDS-PAGE and transferred to nitrocellulose membranes. Membranes were blocked in PBS-tween buffer (PBST, 0.05% v/v) containing 3% skim milk and incubated overnight at 4°C with the corresponding primary antibodies to the following: eukaryotic initiation factor 3 subunit b (eIF3/p116), 1:1000 (Biolegend), methyl tetrahydrofolate reductase 1 (MTHF1), 1:1000 (Santa Cruz). After washing with PBST, membranes were incubated with HRP-conjugated secondary antibodies (Santa Cruz) for 1 h at room temperature, and specific proteins were visualized by enhanced chemiluminescence detection.

Matrigel invasion assay

Invasion assay was performed using Matrigel in 24-well plates, as per manufacturer´s instructions. Briefly, Matrigel was mixed with culture media (1:1) and 200 µl of the mixture was placed in each well and polymerized for 30 min at 37°C. A suspension of 5x10^4 cells previously exposed to Ch-SeNPs (0.5 and 1 µg/ml for 48h) was added to the bottom of the well. Invasion of HepG2 cells was observed after incubation at 37°C for 5 h by phase-contrast microscopy.

Protein identification and quantitation

HepG2 cells were grown in either 'light' (^{12}C$_6$-Lys and ^{12}C$_6$-Arg) or 'heavy' (^{13}C$_6$-Lys and ^{13}C$_6$-Arg) DMEM medium containing 10% dialyzed FBS and 100 units/ml of penicillin/streptomycin. Cells were grown for at least six doublings to allow full incorporation of labeled amino acids. Two large-scale SILAC replicates (10^7 cells per condition) were performed. Complete incorporation of ^{13}C$_6$-Lys and ^{13}C$_6$-Arg after six cell divisions in isotopically heavy medium was verified by MS of a protein digest. Cells labeled with "heavy" (direct SILAC) or "light" (reversed SILAC) amino acids were exposed to 1 µg ml^{-1} Ch-SeNPs for 48 hours. Cells grown with "heavy" and "light" medium were mixed in a 1:1 ratio before subsequent processing. Cells were lysed in a buffer containing 1% Triton X-100, 150 mM NaCl, 20 mM Tris, pH

8, 0.2 mM ethylene diamine tetraacetic acid (EDTA), 2 mM Na_3VO_4, 2 mM NaF, and protease inhibitors (Complete tablet; Roche). Proteins were then separated by SDS-PAGE on 10% SDS-polyacrylamide gels. After electrophoresis, the proteins were visualized by Coomassie blue staining and in-gel digested as previously described [13].

The peptide mixtures from the different in-gel tryptic digestion fractions were loaded onto a trap column (Reprosil C18, 3 μm particle size, 0.3 x 10 mm, 120 Å pore size, SGE) and then eluted to the analytical column (Acclaim PepMap 100, C18, 3 μm particle size, 75 μm x 150 mm, 100 Å pore size, Dionex, LC Packings) with a linear gradient of 5-95% ACN in 0.1% formic acid. The samples were delivered over 120 min by a nano-LC ultra 1D plus system (Eksigent) at a flow-rate of 200 nl/min, through the analytical column to a stainless steel nano-bore emitter (O.D. 150 um, I.D. 30 um Proxeon, Odense, Denmark). The peptides were scanned and fragmented with an LTQ XL linear ion trap mass spectrometer (Thermo Scientific, San Jose, CA) operated in data-dependent ZoomScan and MS/MS switching mode using the three most intense precursors detected in a survey scan from 400 to 1600 u (three μscans). ZoomScan mass window was set to 12 Da enabling monitoring of the entire $^{12}C/^{13}C$ isotopic envelope of most doubly and triply charged peptides. Singly charged ions were excluded for MS/MS analysis. Normalized collision energy was set to 35% and dynamic exclusion was applied during 3 min periods to avoid repetitive fragmentation of ions.

Generated raw files were converted to mgf files (Bioworks 3.3.1) for submission to the MASCOT database. A database containing the NCBInr *Homo Sapiens* sequences (as of November 2012, 35586 sequences) was searched using the MASCOT protein identification software (v2.3 Matrix Science). Search criteria included trypsin specificity with one missed cleavage allowed, and with methionine oxidation, $^{13}C_6$-Arg and $^{13}C_6$ –Lys as variable modifications. Minimum precursor and fragment-ion mass accuracies of 1.2 and 0.3 Da were used. To consider a protein as an accurate identification, at least one unique peptide (bold-red peptides meaning highest scoring peptide matching to protein with highest total score) with a Mascot score higher than 39 (p<0.05) and a minimum total protein score of 46 (p<0.01) were required. The false positive rate was calculated by searching the same spectra against the NCBInr *Homo sapiens* decoy database. Relative quantification ratios of identified proteins based on peak area were calculated using Quixot v.1.3.26 open-source software (http://150.244.205.155/mediawiki/index.php/QuiXot). Protein ratios obtained by Quixot were verified manually for all peptides. Functional processes and subcellular localization of the proteins identified by SILAC were assigned based on the biological knowledge available in Gene Ontology (GO) annotations.

Results

Synthesis, characterization and cytotoxicity of Ch-SeNPs

We used transmission electron microscopy (TEM) to characterize the synthesized Ch-SeNPs under different concentrations of chitosan in terms of particle size, morphology and aggregation. In all cases, Ch-SeNPs presented a spherical structure with particle size between 10 nm to 60 nm. However, the size distribution was significantly affected by the concentration of chitosan. 0.1% chitosan provided a homogeneous dispersion in which around 80-90% of the Ch-SeNPs had a size in the range 40-60 nm (Figure 1A) and thus, we selected this concentration for further experiments.

Figure 1B shows the viability of HepG2 cells exposed to different concentrations of Ch-SeNPs, Se IV and the synthesis media during 48 h. Cell viability decreased with increasing NPs concentration and exposure times. While the higher concentrations of Ch-SeNPs and Se IV concentrations caused an almost 100% decrease on cell viability, the lowest concentration did not significantly affect cell. In order to evaluate the effect of Ch-SeNPs but without drastically compromising the cell viability, we selected 1 μg ml^{-1} Ch-SeNPs for further experiments. Our data also pointed out that there were only a slight decreased in the viability of cells exposed to Se IV as compared to Ch-SeNPs and that the synthesis media (containing chitosan and ascorbic acid) did not significantly affect the viability of the cells.

Flow cytometry assays

Figure 2A shows the data obtained from flow cytometry analyses regarding the degree of apoptosis and necrosis in cells exposed to Ch-SeNPs and Se IV. We did not observe significant differences in the number of apoptotic or necrotic cell populations between control and cells exposed to Ch-SeNPs. However, cells exposed to Se IV showed a significant increase in apoptotic cells. We also used flow cytometry to further investigate the influence of Ch-SeNPs and Se IV exposure on the cell cycle patterns of HepG2 cells by measuring the content of DNA (Figures 2B and 2C). After exposure to Ch-SeNPs, the number of cells in G0/G1 decreased to the same point that the populations in S-G2/M increased. The number of cells in sub-G0 (apoptotic cells) significantly increased in cells exposed to Se IV, thus confirming the apoptosis assay.

Cellular uptake and localization of Ch-SeNPs

We determined the total Se content in the cell culture media, in the PBS washing solution and in the pellet of cells exposed to 1 μg ml^{-1} Ch-SeNPs for 48 h by ICP-MS. The data obtained showed that the majority of Se was found in the culture media and that only 1% of the total Se added was internalized by the cells after 48 h. Then we used TEM for investigating the cellular localization of Ch-SeNPs. As shown in Figure 3, Ch-SeNPs were uptaken by HepG2 cells, localized in vacuoles (Figure 3A), also distributed throughout the cytoplasm (Figure 3B) and in subcellular organelles such as mitochondria and the endoplasmic reticulum (ER) (Figures 3C and 3D). In addition, about 90% of cells exposed to Ch-SeNPs exhibit more than 2-fold increase in the number of vacuoles as compared to control cells (Figures 3E and 3F).

Quantitative proteomics

To identify the proteins altered after Ch-SeNPs exposure, we performed two large-scale SILAC experiments (Figure 4A). Mass spectrometry analysis identified a total of 1170 proteins with at least one unique peptide in the two SILAC experiments and a false discovery rate of 0.4% estimated from the number of hits against the reverse sequence/total hits ratio, p>0.01. However, only 650 proteins passed the criteria established for protein quantitation, which include identification of at least two unique peptides with a MASCOT score >39 for the peptides and >46 for the full protein. Out of these proteins, 481 were found in both replicates (Supplementary Information, Table S1). The global overlap between the two SILAC experiments was 69%. We then focused on proteins with at least 1.3-fold difference between control and exposed cells and with 20% as the maximum relative standard deviation between peptides within each protein. Most of the identified proteins had a SILAC ratio close to 1. Judge by this criteria, 41 proteins were considered significantly altered in Ch-SeNPs exposed HepG2 cells compared with control cells. Of these, 21 were up-regulated and 20 down-regulated (Table 1).

For an unbiased search of pathways involved in Ch-SeNPs exposure, we submitted the 41 altered proteins to knowledge-based

Accession number (gi)	Protein name	Common name	Mascot score	SILAC ratio	RSD[a]
94721250	VAMP (vesicle-associated membrane protein)-associated protein A, 33kDa	VAPA	275	2.75	5.02
167466173	heat shock 70kDa protein 1A	HSPA1A/HSPA1B	558	1.84	8.41
24307969	cytoplasmic FMR1 interacting protein 1	CYFIP1	171	1.65	16.83
4504041	guanine nucleotide binding protein (G protein), alpha inhibiting activity polypeptide 2	GNAI2	128	1.65	8.10
4757756	annexin A2	ANXA2	144	1.55	4.24
4826898	profilin 1	PFN1	46	1.51	16.24
28557709	phosphoribosyl pyrophosphate synthetase 1-like 1	PRPS1L1	74	1.50	1.86
9910382	translocase of outer mitochondrial membrane 22 homolog	TOMM22	119	1.47	1.44
4557797	non-metastatic cells 1, protein (NM23A) expressed in	NME1	189	1.42	12.59
14141152	heterogeneous nuclear ribonucleoprotein M	HNRNPM	548	1.36	2.28
5901922	cell division cycle 37 homolog	CDC37	151	1.34	11.49
38570062	golgi to ER traffic protein 4 homolog	GET4	52	1.35	0.77
22749415	STT3, subunit of the oligosaccharyltransferase complex, homolog A	STT3A	90	1.35	18.66
4504279	H3 histone, family 3B (H3.3B)	H3F3A/ H3F3B	83	1.34	0.29
42558250	cell cycle associated protein 1	CAPRIN1	98	1.33	3.43
4501857	acyl-CoA dehydrogenase, long chain	ACADL	89	1.33	0.06
20149560	syntaxin 4	STX4	35	1.32	1.03
33519426	thioredoxin reductase 1	TXNRD1	208	1.31	5.53
4503519	eukaryotic translation initiation factor 3, subunit F	EIF3F	314	1.30	8.40
8923390	coiled-coil-helix-coiled-coil-helix domain containing 3	CHCHD3	52	1.30	11.51
4503729	FK506 binding protein 4, 59kDa	FKBP4	195	1.30	15.51
4759302	VAMP (vesicle-associated membrane protein)-associated protein B and C	VAPB	189	-1.32	8.29
23397429	eukaryotic translation initiation factor 3, subunit M	EIF3M	264	-1.32	11.31
4503523	eukaryotic translation initiation factor 3, subunit D	EIF3D	154	-1.32	17.54
71773329	annexin A6	ANXA6	296	-1.33	15.72
18379349	vesicle amine transport protein 1 homolog	VAT1	416	-1.35	12.77
4501867	aconitase 2, mitochondrial	ACO2	124	-1.37	18.76
148491070	CTP synthase	CTPS	171	-1.37	14.43
223468663	aldo-keto reductase family 1, member B10 (aldose reductase)	AKR1B10	97	-1.41	10.77
13491174	MARCKS-like 1	MARCKSL1	122	-1.43	17.02
148727247	ubiquitin specific peptidase 5 (isopeptidase T)	USP5	96	-1.43	12.95
4757732	apoptosis-inducing factor, mitochondrion-associated, 1	AIFM1	131	-1.45	4.65
112363070	HSPA (heat shock 70kDa) binding protein, cytoplasmic cochaperone 1	HSPBP1	61	-1.47	19.94
91807122	annexin A8-like 2	ANXA8L2	497	-1.52	16.28
24308514	glutathione S-transferase alpha 5	GSTA5	57	-1.52	10.70
109134349	coatomer protein complex, subunit gamma 2	COPG2	132	-1.52	5.84
4506619	ribosomal protein L24	RPL24	71	-1.54	8.89
4503243	cytochrome P450, family 51, subfamily A, polypeptide 1	CYP51A1	355	-1.54	7.32
100913206	DEAH (Asp-Glu-Ala-His) box polypeptide 9	DHX9	179	-1.54	17.86
62241042	glutamyl-prolyl-tRNA synthetase	EPRS	95	-1.61	17.68
5453990	proteasome (prosome, macropain) activator subunit 1 (PA28 alpha)	PSME1	435	-2.27	11.86

[a]Relative standard deviation

Table 1: Differentially expressed proteins in HepG2 Cells after exposure with 1 μg ml⁻¹ of Ch-SeNPs.

Ingenuity pathway analysis (IPA). This allowed us to identify enriched canonical pathways involved in cell growth, cell proliferation, protein synthesis, DNA replication, nucleic acid metabolism, post-translational modification and cellular death. We also classified the differentially expressed proteins to their molecular and cellular functions using the gene ontology (GO) database. We found altered proteins involved in cell cycle regulation, cellular compromise, cellular growth and proliferation, amino acid metabolism and cell morphology (Figure 4B).

Fluorescence microscopy inspection of eIF3a and eIF3b levels

Figure 5 shows the fluorescence microscopy images of HepG2 cells (control and exposed to 1.0 μg ml⁻¹ Ch-SeNPs) prior an immunofluorescence assay to evaluate the level of expression of eIF3a and eIF3b subunits. The expression of both subunits appeared significantly inhibited after exposure to Ch-SeNPs for 48 h. These

results are in agreement with the proteomic data obtained and suggest that exposure to Ch-SeNPs inhibit the levels of expression of the eIF3 complex.

eIF3 silencing

To support the idea that the mechanism by which Ch-SeNPs induce cell cycle arrest at the S phase is by inhibiting the expression of most subunits of the eIF3 complex, thus affecting the protein synthesis machinery, we investigated whether siRNA-mediated gene knockdown of the eIF3b subunit induces cell cycle arrest in a similar manner to Ch-SeNPs exposure in HeLa cells. After validating the suitability of the transfection (Figure 6A) by Western Blot, we analyzed the cell cycle pattern of transfected cells and cells exposed to Ch-SeNPs by flow cytometry (Figure 6B). Silencing of the eiF3b expression partially increased the cell population in S-G2/M phase while decreased the
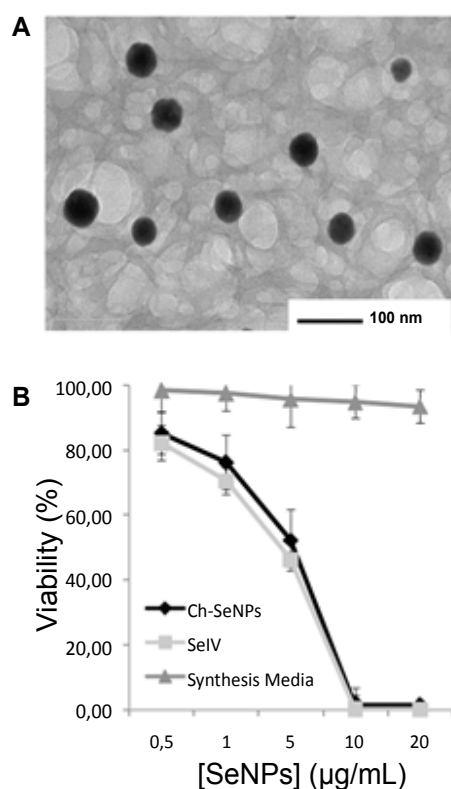
Figure 1: The use of 0.1% chitosan as stabilizer provided a homogeneous SeNPs suspension with around 80-90% of NPs in the range 40-60 nm. Cell viability of HepG2 cells exposed to Ch-SeNPs and Se IV decreased in a dose-dependent manner.
(A) Transmission electron microscopy of Ch-SeNPs synthesized in the presence of 0.1% chitosan.
(B) Cell viability of HepG2 cells exposed to different concentrations of Ch-SeNPs, Se IV and the synthesis media. The MTT assay showed that high concentrations (10-20 μg ml^{-1} of Ch-SeNPs and Se IV) caused an almost 100% decrease in the cell viability. Exposure conditions of 1 μg ml^{-1} of Ch-SeNPs induced a 30% decrease in cell viability and were selected for further experiments.

population in the G0/G1 phase. The differences observed as compared to control cells, were similar to those obtained after Ch-SeNPs exposure.

Matrigel assay

Figure 6C, shows the invasive behavior of HepG2 cells over matrigel cell culture. We observed that control cells migrated over the surface of matrigel forming large cellular branches, whereas cells exposed to 0.5 μg ml^{-1} Ch-SeNPs formed a less branched culture. The invasive behavior decreased with increasing concentrations of Ch-SeNPs and in fact, the morphology of cells exposed to 1.0 μg ml^{-1} Ch-SeNPs was very different from control cells, appearing round and individuals with no ramifications.

Discussion

In a previous report, Bai et al. demonstrated the capability of monosaccharides (glucose), oligosaccharides (sucrose) and polysaccharides (chitosan) to modify the size, morphology and stability of SeNPs in liquid dispersions. We used chitosan since previous studies have shown how encapsulation of Se IV into chitosan significantly improved the antioxidant properties and promoted a high retention of selenium in cells [12]. We observed that the size distribution of

NPs was significantly affected by the concentration of polysaccharide used in synthesis reaction. 0.1% chitosan was the best concentration in terms of nanoparticles diameter and size distribution (Figure 1A). We did not observed significant differences in the TEM images as for changes in particle size and aggregation for Ch-SeNPs stored at 4°C for up to 2 months. Moreover, no flocculation was visually detected. We also examined the potential oxidation of Ch-SeNPs to Se IV weekly by centrifugation of the Ch-SeNPs suspension using 10 KDa cut-off filter. The total Se present in the liquid fraction was quantified by ICP-MS. We only found a low percentage of ionic Se (< 0.1%), thus showing the good stability of the synthesized Ch-SeNPs.

Ch-SeNPs induce cell cycle arrest

The viability of cells exposed to either Ch-SeNPs or Se IV decreased in a similar concentration-dependent manner (Figure 1B). However, we visually observed that while cells exposed to Ch-SeNPs seemed to have stopped dividing, cultures exposed to Se IV presented a significant number of dead floating cells. In order to confirm these differential effects, we carried out flow cytometry to evaluate both, apoptosis and cell cycle pattern. It is important to mention that the synthesis media composed by chitosan, ascorbic and acetic acid did not significantly influence the viability of HepG2 cells, which confirm that the effect observed in cells exposed to Ch-SeNPs was due to Ch-SeNPs themselves

Flow cytometry confirmed that the percentage of apoptotic or necrotic cell populations in cells exposed to Ch-SeNPs was not significantly different from control cells (Figure 2A), which correlates well with the absence of chromosome condensation and nuclear fragmentation, typical features for apoptotic cells, in our TEM images (Figure 3). However, cells exposed to Se IV presented a significant percentage of apoptotic cells, thus showing the higher toxicity exerted by Se IV as compared to Ch-SeNPs at this concentration.

We also investigated the influence of these NPs on the cell cycle patterns of HepG2 cells. The decrease of cell population in G0/G1 phase along with the increase in S-G2/M suggest that Ch-SeNPs induce cell cycle arrest at the S phase (Figures 2B and 2C), which is in agreement with a previous study carried out on HeLa and MDA-MB-231 cells [7]. In addition, a significant cell population of cells exposed to Se IV was found in the sub-G0 phase (Figure 2B), which is consistent with the apoptosis assay.

The data derived from the flow cytometry analyses supported the different effect induced by Ch-SeNPs in arresting the cell cycle of HepG2 cells as compared to the effect of Se IV, which, in contrast, induced apoptosis at the same tested concentration.

Internalization of Ch-SeNPs

When performing an *in vitro* study, the degree of cellular internalization is a potentially relevant factor for understanding the biological mechanisms affected by Ch-SeNPs exposure. Many authors have reported a close correlation between intracellular uptake and cytotoxic effects [14]. Our ICP-MS analysis showed that only 1% of Se was internalized after 48 h. These results showed how even small amounts of Ch-SeNPs could greatly alter cell functioning. We then used TEM for cellular localization of the internalized Ch-SeNPs with two purposes: (i) to discard the possibility of potential oxidation of Ch-SeNPs in contact with the cells or the culture media; and (ii) to confirm whether or not the Ch-SeNPs were really inside the cells or just attached to the cell membranes. Our TEM images showed Ch-SeNPs localized in vacuoles (Figure 3A), distributed throughout the cytoplasm (Figure 3B) and in subcellular organelles such as mitochondria and the
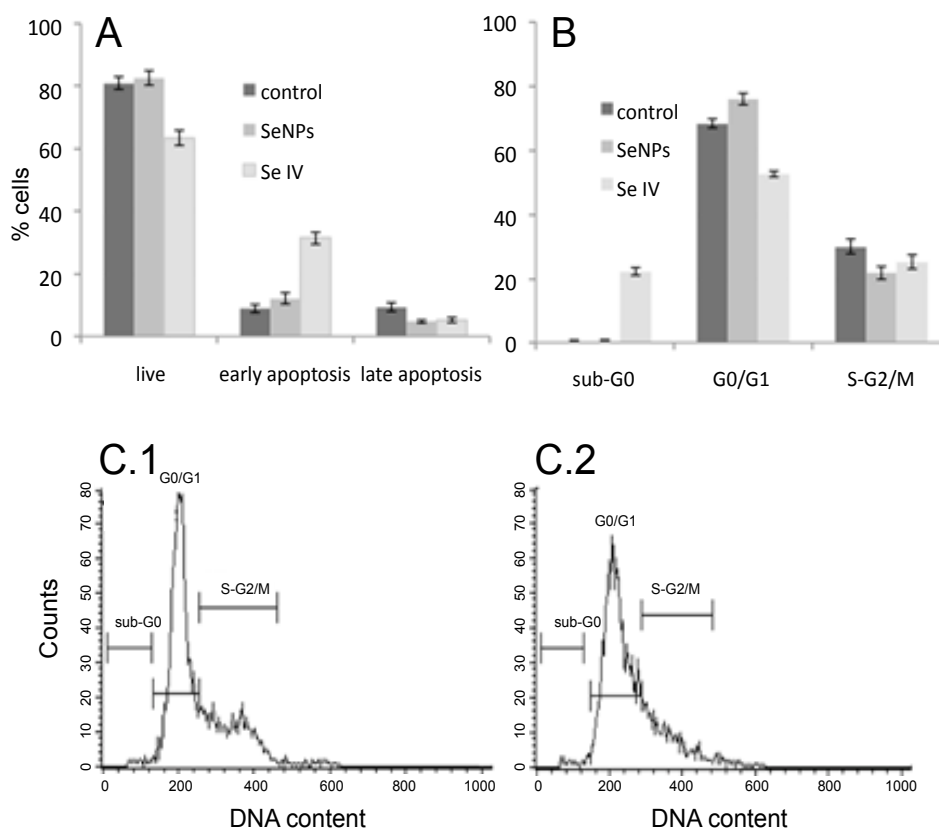
Figure 2: Ch-SeNPs exposure of HepG2 cells did not induce apoptosis but a cell cycle arrest at the S phase.
(A) Annexin-V-based flow cytometry analysis did not reveal a significant increase in apoptosis after Ch-SeNPs exposure. Se IV, in contrast, induce a significant increase of apoptotic cells.
(B) Measurement of the DNA content by flow cytometry of Ch-SeNPs-exposed cells showed that the number of cells in G0/G1 decrease to the same point that the populations in S-G2/M increase (C1) as compared to control cells (C2).
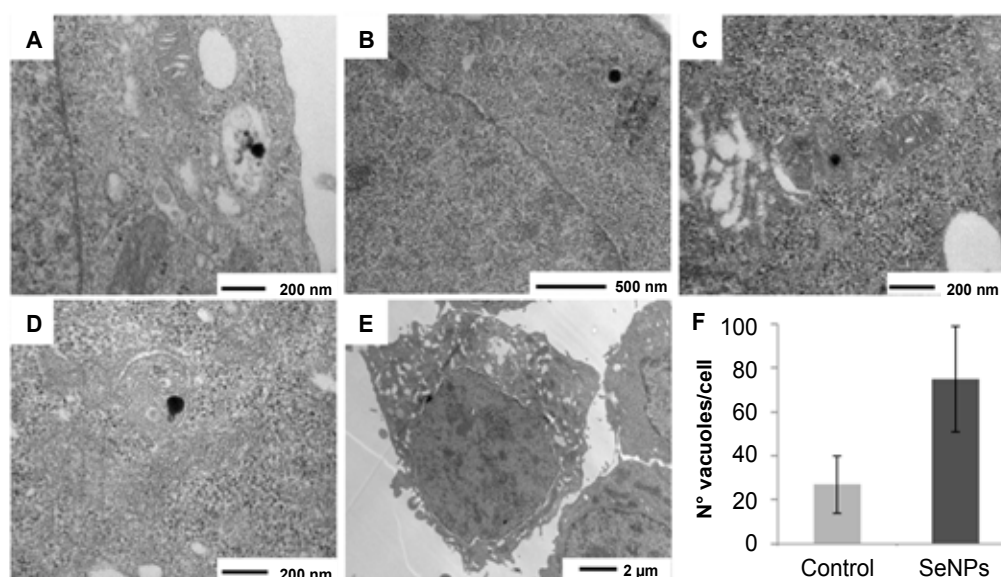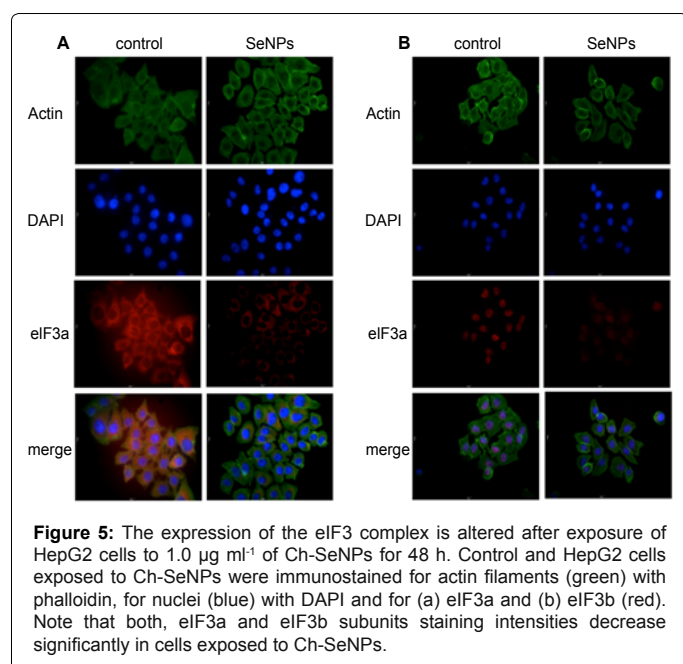

Figure 3: Transmission electron microscopy showed that Ch-SeNPs uptaked by HepG2 cells are localized in (A) vacuoles, (B) throughout the cytoplasm and in subcellular organelles such as (C) mitochondria and (D) the endoplasmic reticulum. As expected, Ch-SeNPs were not localized in the nuclei due to their particle size.
(E, F) About 90% of cells exposed to Ch-SeNPs exhibit more than 2-fold increased in the number of vacuoles as compared to control cells.

Figure 4: (A) A quantitative proteomic approach based on stable isotopic labeling by amino acids in cell culture (SILAC) identified a set of de-regulated proteins upon Ch-SeNPs exposure. (B) Altered proteins were involved in cell cycle regulation (RCC), cellular compromise (CC), cellular growth and proliferation (CGP), amino acid metabolism (AAM) and cell morphology (CM). Among these found de-regulated proteins, several subunits of the eIF3 protein complex, involved in the protein synthesis machinery, appeared down-regulated after Ch-SeNPs exposure.

Figure 5: The expression of the eIF3 complex is altered after exposure of HepG2 cells to 1.0 µg ml^{-1} of Ch-SeNPs for 48 h. Control and HepG2 cells exposed to Ch-SeNPs were immunostained for actin filaments (green) with phalloidin, for nuclei (blue) with DAPI and for (a) eIF3a and (b) eIF3b (red). Note that both, eIF3a and eIF3b subunits staining intensities decrease significantly in cells exposed to Ch-SeNPs.

endoplasmic reticulum (ER) (Figures 3C and 3D). These two organelles play an important role in different processes including cellular energy supplying, differentiation and apoptosis [15]. As expected, Ch-SeNPs were not localized in the nuclei due to their particle size, thus reducing the possibility of DNA damage. In addition, a massive vacuolization was visualized in 90% of cells treated with Ch-SeNPs (Figures 3E and 3F). These results agree well with a previous study where formation of membrane fusion vesicles during active endocytosis was induced in breast adenocarcinoma cells exposed to SeNPs [16].

Ch-SeNPs exposure affects the expression of the eIF3 protein complex

After assessing the ability of Ch-SeNPs to induce cell cycle arrest, we used a quantitative proteomic approach for identifying differentially expressed proteins in control vs. Ch-SeNPs-exposed cells in order to gain a deeper insight into the biomolecular mechanisms involved. Our SILAC experiment reported the alteration of proteins involved in cell growth, cell development and protein synthesis by Ch-SeNPs exposure, which may be closely related with the cell cycle inhibitory effect observed in exposed HepG2 cells (Figure 4B). Protein synthesis is closely integrated with other metabolic pathways, influencing transcription, protein turnover and early development. Among the de-regulated proteins found in our SILAC experiments, we identified down-regulated two eukaryotic translation initiation factor 3 (eIF3) subunits (eIF3m and EiF3d). The eIF3 complex, formed by thirteen protein subunits, is considered the largest of the initiation factors, since the regulation of the protein synthesis and protein degradation machinery is coordinated through some eIF3 subunits [17]. eIF3 has two main roles in protein synthesis: first, eIF3 binds to the 40S ribosome and facilitates loading of the Met-tRNA/eIF2·GTP ternary complex to form the 43S pre-initiation complex; and secondly, eIF3 apparently assists eIF4 in recruiting mRNAs to the 43S complex [18].

The subunit eIF3m is associated to different mRNAs encoding proteins involved in nucleic acid metabolism, transporter proteins and proteins of unknown function [19]. It has been observed that the eIF3m subunit is highly expressed in many human cancer cell lines and its overexpression can be related to tumor progression. In addition, down-regulation of eIF3m reduces the proliferation of carcinogenic cells. Goh et al. silenced the expression of the eIF3m subunit by specific siRNA and confirmed the influence of eIF3m on cell proliferation, cell cycle progression and cell death in human colon cancer cell line HCT-116 by decreasing the CDC25A activity, which is required for progression from G1 to the S phase of the cell cycle [20]. Based on the evidences reported in previous studies, and the down-regulation of the eIF3m and eIF3d subunits observed in our SILAC approach after Ch-SeNPs exposure, we hypothesized that the inhibition of the expression of the eIF3 complex could be directly related with the inhibitory effect of Ch-SeNPs on the proliferation of HepG2 cells.

Another subunit, eIF3a, involved in cell proliferation and tissue development has also been found highly overexpressed in several human and murine cancer tissues [21,22]. In fact, many studies have reported the role of eIF3a as an early differentiation marker in human mammary carcinoma cells, although the role of this subunit in oncogenesis is still unclear. The eIF3b subunit is considered to be the major scaffolding subunit [23] and has an important role in human glioblastoma development [24]. In addition, it has been suggested that the protein synthesis machinery can be significantly inhibited in human colorectal cancer cells by decreasing the expression of the eIF3b subunit [25]. Since we did not identify either the eIF3a or the eIF3b subunit in our SILAC approach, we performed an immunofluorescence assay to evaluate the level of expression of these subunits after exposure to Ch-SeNPs (Figure 5). The expression of both subunits appeared significantly inhibited after exposure of HepG2 cells to Ch-SeNPs. These findings support the proteomic data obtained and suggest that exposure to Ch-SeNPs inhibit the levels of expression of the eIF3 complex, which is closely related to the inhibition of cell proliferation.

Unlike the other subunits, we found eIF3f overexpressed in our SILAC approach. Although this result may sound contradictory with our previous conclusions, interestingly, eIF3f is involved in the development and apoptosis of tumor cells by interaction with CDK11 [26]. In fact, it has been demonstrated that eIF3f appeared down-regulated in most human tumors and its ectopic expression inhibited translation and cellular protein synthesis in pancreatic cancer cells,
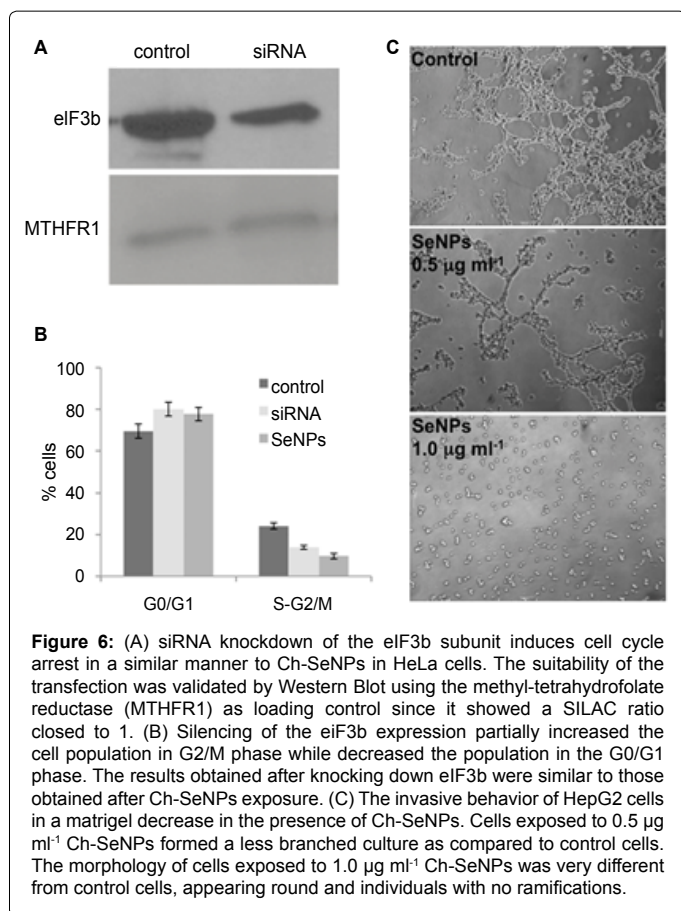
Figure 6: (A) siRNA knockdown of the eIF3b subunit induces cell cycle arrest in a similar manner to Ch-SeNPs in HeLa cells. The suitability of the transfection was validated by Western Blot using the methyl-tetrahydrofolate reductase (MTHFR1) as loading control since it showed a SILAC ratio closed to 1. (B) Silencing of the eiF3b expression partially increased the cell population in G2/M phase while decreased the population in the G0/G1 phase. The results obtained after knocking down eIF3b were similar to those obtained after Ch-SeNPs exposure. (C) The invasive behavior of HepG2 cells in a matrigel decrease in the presence of Ch-SeNPs. Cells exposed to 0.5 µg ml^{-1} Ch-SeNPs formed a less branched culture as compared to control cells. The morphology of cells exposed to 1.0 µg ml^{-1} Ch-SeNPs was very different from control cells, appearing round and individuals with no ramifications.

inducing them to enter apoptosis [27]. The fact that we found eIF3f up-regulated while other eIF3 subunits were down-regulated strongly support the idea that Ch-SeNPs induce cell cycle arrest at the S phase mediated by de-regulation of most subunits of the eIF3 complex, thus affecting the protein synthesis machinery. This hypothesis was investigated by silencing eIF3b subunit through a transfection assay. The similar cell cycle pattern among transfected cells and cells exposed to Ch-SeNPs (showing a slight increased of cell population in S-G2/M phase and a decreased of cells in G0/G1 phase) together with the different level of expression found for eIF3 subunits after Ch-SeNPs exposure that we showed previously, support the hypothesis that Ch-SeNPs induce eIF3-mediated cell cycle arrest (Figures 6A and 6B).

Differentially expressed proteins upon Ch-SeNPs exposure

In addition to some of the subunits of the eIF3 protein complex, we found other proteins altered in our SILAC approach that could also help to better understand the mechanisms involved in the cell interaction with Ch-SeNPs. One of the proteins that showed a higher up-regulation after Ch-SeNPs exposure was the VAPA (VAMP (vesicle-associated membrane protein)-associated protein A) protein. VAPs proteins are endoplasmic reticulum (ER)-resident membrane proteins that are broadly expressed in eukaryotic cells and are involved in stress signaling, membrane trafficking and ER homeostasis [28]. VAPA is related to the lateral diffusion inhibition of membrane proteins, and also is associated with intracellular vesicles so that the massive vacuolization found in cells exposed to Ch-SeNPs (Figure 3F) could be induced by VAPA up-regulation [29]. It has been reported that over expression of the VAPA isoform but not the B isoform (VAPB) inhibited ER-to-Golgi

transport of membrane proteins. Interestingly, we found VAPB slightly down-regulated suggesting that this protein may also be involved in the pathway through which Ch-SeNPs inhibited protein synthesis.

Heat shock proteins (HSPs) constitute a group of chaperone proteins that play a pivotal role in the maintenance of protein homeostasis. In our SILAC approach, the expression of heat shock 70 kDa protein 1A (HSPA1A/HSPA1B) was highly up-regulated. This result is in agreement with previous studies in which HSP70 was dramatically up-regulated under environmental stress [30].

Cell division cycle 37 homolog (CDC37), a positive regulator of stability and/or activity of some protein kinases, appeared up-regulated in our experiment. This protein is involved in SAPK regulation, a stress-activated protein kinase dedicated to transmit environmental stress stimuli, which has a crucial role in cellular survival under stress conditions and inflammatory responses [31]. It is also worth mentioning that mammalian SAPK is related with the response of cancer cells to cytotoxic treatments [32].

Cytoplasmic FMR1 interacting protein 1 (Cyfip1) has been defined as a potential tumor suppressor that regulates invasive behavior. The loss of CYFIP1 expression has been correlated with tumor progression in epithelial and colon cancers [33]. Interestingly, we found this protein over-expressed after Ch-SeNPs exposure, thus showing the capability of Ch-SeNPs to raise the expression levels of certain tumor suppressors, such as in the case of the eIF3f subunit previously shown.

The apoptosis-inducing factor mitochondrion-associated 1 (AIF1) is involved in apoptosis because it induces the mitochondria to release cytochrome c and caspase-9. Down-regulation of AIF1 has been associated with low apoptosis ratio [34]. Interestingly, AIF1 appeared down-regulated after Ch-SeNPs exposure in our SILAC approach, which correlates well with the fact that no apoptosis was observed in cells exposed to Ch-SeNPs (Figure 2A).

Ch-SeNPs inhibit in-vitro invasiveness of HepG2 cells

We used matrigel cell culture, which has been widely used for in vitro studies on tumor growth [35], in order to evaluate the capacity of Ch-SeNPs to preclude cell invasion. It is known that the differentiation response on matrigel is dependent on the cell type being easily distinguished malignant and non-malignant cells by their morphology when they are cultured on the surface of this basement membrane matrix [36]. The images obtained under phase contrast microscopy (Figure 6C) showed that the exposure to Ch-SeNPs has a negative effect on invasive behavior of HepG2 cells. It can be observed how cells exposed to Ch-SeNPs appeared round and individuals with no ramifications as in the case of control cells.

Conclusions

To the best of our knowledge, this is the first time that a quantitative proteomic approach has been used to unravel the molecular mechanisms underlying the effects induced by SeNPs in cultured hepatocarcinoma cells. In summary, our data strongly suggest that the cell cycle of HepG2 cells is arrested at the S phase by alteration of the eIF3 protein complex expression as result of Ch-SeNPs exposure, which may hampers translation of mRNAs responsible for encoding proteins important for cell proliferation and oncogenesis. We have shown by different independent approaches how different eIF3 subunits, which are commonly found up-regulated in several types of tumors, are down-regulated after Ch-SeNPs exposure, except for eIF3f, which is the only eIF3 subunit that has been proposed as tumor suppressor and therefore

may also contribute to attenuate cell proliferation. In addition, we have demonstrated the ability of Ch-SeNPs to inhibit *in vitro* cell invasion and the de-regulation of other proteins that could also be involved in the overall inhibition of cell proliferation induced by Ch-SeNPs.

Acknowledgment

References

1. Fairweather-Tait SK, Bao Y, Broadley MR, Collings R, Ford D, et al. (2011) Selenium in human health and disease. Antioxid Redox Signal 14: 1337-1383.

2. Abdulah R, Miyazaki K, Nakazawa M, Koyama H (2005) Chemical forms of selenium for cancer prevention. J Trace Elem Med Biol 19: 141-150.

3. Wang H, Zhang J, Yu H (2007) Elemental selenium at nano size possesses lower toxicity without compromising the selenoenzymes: comparison with selenomethionine in mice. Free Radic Biol Med 42: 1524-1533.

4. Zhang J, Wang X, Xu T (2008) Elemental selenium at nano size (nano-Se) as a potential chemopreventive agent with reduced risk of selenium toxicity: comparison with Se-methylselenocysteine in mice. Toxicol Sci 101: 22-31.

5. Jin-Song Z, Xue-Yun G, Li-De Z, Yong-Ping B (2001) Biological effects of a nano red elemental selenium. Biofactors 15: 27-38.

6. Chen T, Wong YS, Zheng W, Bai Y, Huang L (2008) Selenium nanoparticles fabricated in *Undaria Pinnatifida* polysaccharide solutions induce mitochondria-mediated apoptosis in A375 human melanoma cells. Colloids Surf B Biointerfaces 67: 26-31.

7. Luo H, Wang F, Bai Y, Chen T, Zheng W (2012) Selenium nanoparticles inhibit the growth of HeLa and MDA-MB-231 cells through induction of S phase arrest. Colloids Surf B Biointerfaces 94: 304-308.

8. Estevez H, Garcia-Lidon JC, Luque-Garcia JL, Camara C (2014) Effects of chitosan-stabilized selenium nanoparticles on cell proliferation, apoptosis and cell cycle pattern in HepG2 cells: Comparison with other selenospecies. Colloids Surf B Biointerfaces 122C: 184-193.

9. Luque-Garcia JL, Cabezas-Sanchez P, Camara C (2011) Proteomics as a tool for examining the toxicity of heavy metals. Trends Anal Chem 30: 703-716.

10. Cuello S, Ramos S, Madrid Y, Luque-Garcia JL, Camara C (2012) Differential protein expression of hepatic cells associated with MeHg exposure: deepening into the molecular mechanisms of toxicity. Anal Bioanal Chem 404: 315-324.

11. Ren Y, Zhao T, Mao G, Zhang M, Li F, et al. (2013) Antitumor activity of hyaluronic acid-selenium nanoparticles in heps tumor mice models. Int J Biol Macromol 57: 57-62.

12. Bai Y, Wang Y, Zhou Y, Li W, Zheng W (2008) Modification and modulation of saccharides on elemental selenium nanoparticles in liquid phase. Materials Letters 62: 2311-2314.

13. Rivera-Torres J, Acín-Perez R, Cabezas-Sanchez P, Osorio FG, Gonzalez-Gomez C, et al. (2013) Identification of mitochondrial dysfunction in Hutchinson-Gilford progeria syndrome through use of stable isotope labeling with amino acids in cell culture. J Proteomics 91: 466-477.

14. Zhang M, Li J, Xing G, He R, Li W, et al. (2011) Variation in the internalization of differently sized nanoparticles induces different DNA-damaging effects on a macrophage cell line. Arch Toxicol 85: 1575-1588.

15. Green DR, Reed JC (1998) Mitochondria and apoptosis. Science 281: 1309-1312.

16. Huang Y, He L, Liu W, Fan C, et al. (2013) Selective cellular uptake and induction of apoptosis of cancer-targeted selenium nanoparticles. Biomaterials 34: 7106-7116.

17. Harris TE, Chi A, Shabanowitz J, Hunt DF, et al. (2006) mTOR-dependent stimulation of the association of eIF4G and eIF3 by insulin. EMBO J 25: 1659-1668.

18. Siridechadilok B, Fraser CS, Hall RJ, Doudna JA, Nogales E (2005) Structural roles for human translation factor eIF3 in initiation of protein synthesis. Science 310: 1513-1515.

19. Zhou C, Arslan F, Wee S, Krishnan S, Ivanov AR, et al. (2005) PCI proteins eIF3e and eIF3m define distinct translation initiation factor 3 complexes. BMC Biol 3: 14-29.

20. Gosh SH, Hong SH, Lee BC, Ju MH, Jeong JS, et al. (2011) eIF3m expression influences the regulation of tumorigenesis-related genes in human colon cancer. Oncogene 30: 398-409.

21. Pincheira R, Chen Q, Zhang JT (2001) Identification of a 170-kDa protein over-expressed in lung cancers. Br J Cancer 84: 1520-1527.

22. Liu Z, Dong Z, Yang Z, Chen Q, Pan Y, et al. (2007) Role of eIF3a (eIF3 p170) in intestinal cell differentiation and its association with early development. Differentiation 75: 652-661.

23. Fraser CS, Lee JY, Mayeur GL, Bushell M, Doudna JA, et al. (2004) The j-subunit of human translation initiation factor eIF3 is required for the stable binding of eIF3 and its subcomplexes to 40S ribosomal subunits in vitro. J Biol Chem 279: 8946-8956.

24. Liang H, Ding X, Zhou C, Zhang Y, Xu M, et al. (2012) Knockdown of eukaryotic translation initiation factors 3b (eIF3b) inhibits proliferation and promotes apoptosis in glioblastoma cells. Neurol Sci 33: 1057-1062.

25. Wang Z, Chen J, Sun J, Cui Z, Wu H (2012) RNA interference-mediated silencing of eukaryotic translation initiation factor 3, subunit b (eIF3b) gene expression inhibits proliferation of colon cancer cells. World J Surg Oncol 10: 119-127.

26. Beyaert R, Kidd VJ, Cornelis S, Van de Craen M, Denecker G, et al. (1997) Cleavage of PITSLRE kinases by ICE/CASP-1 and CPP32/CASP-3 during apoptosis induced by tumor necrosis factor. J Biol Chem 272: 11694-11697.

27. Shi J, Kahle A, Hershey JWB, Honchak BM, Warneke JA, et al. (2006) Decreased expression of eukaryotic initiation factor 3f deregulates translation and apoptosis in tumor cells. Oncogene 25: 4923-4936.

28. Amarillo R, Ramachandran S, Sabanay H, Lev S (2005) Differential regulation of endoplasmic reticulum structure through VAP-Nir protein interaction. J Biol Chem 280: 5934-5944.

29. Prosser DC, Tran D, Gougeon PY, Verly C, Ngsee JK (2008) FFAT rescues VAPA-mediated inhibition of ER-to-golgi transport and VAPB-mediated ER aggregation. J Cell Biol 121: 3052-3061.

30. De Maio A (1999) Heat shock proteins: facts, thoughts, and dreams. Shock 11: 1-12.

31. Tatebe H, Shiozaki K (2003) Identification of Cdc37 as a novel regulator of the stress-responsive mitogen-activated protein kinase. Mol Cell Biol 23: 5132-5142.

32. Kyriakis JM, Avruch J (2001) Mammalian mitogen-activated protein kinase signal transduction pathways activated by stress and inflammation. Physiol Rev 81: 807-869.

33. Silva JM, Ezhkova E, Silva J, Heart S, Castillo M, et al. (2009) Cyfip1 Is a Putative Invasion Suppressor in Epithelial Cancers. Cell 137: 1047-1061.

34. Susin SA, Lorenzo HK, Zamzami N, Marzo I, Snow BE, et al. (1999) Molecular characterization of mitochondrial apoptosis-inducing factor. Nature 397: 441-446.

35. Noel A, De Pauw-Gillet MC, Purnell G, Nusgens B, Lapierre CM, et al. (1993) Enhancement of tumorigenicity of human breast adenocarcinoma cells in nude mice by matrigel and fibroblasts. Br J Cancer 68: 909-915.

36. Marques MM, Martins MD, Franca CM (2006) Effect of matrigel on adenoid cystic carcinoma cell line differentiation. Int J Exp Pathol 87: 405-410.